J Sol-Gel Sci Technol (2009) 52:171–178
DOI 10.1007/s10971-009-2023-1

ORIGINAL PAPER

Characterization and preparation of nanocrystalline MgCuZn ferrite powders synthesized by sol–gel auto-combustion method

M. R. Barati

Received: 17 September 2008 / Accepted: 11 June 2009 / Published online: 8 July 2009

Abstract Nanocrystalline Mg–Cu–Zn ferrite powders were successfully synthesized through nitrate–citrate gel auto-combustion method. Characterization of the nitrate–citrate gel, as-burnt powder and calcined powders at different calcination conditions were investigated by using XRD, DTA/TG, IR spectra, EDX, VSM, SEM and TEM techniques. IR spectra and DTA/TGA studies revealed that the combustion process is an oxidation–reduction reaction in which the NO_3^- ion is oxidant and the carboxyl group is reductant. The results of XRD show that the decomposition of the gel indicated a gradual transition from an amorphous material to a crystalline phase. In addition, increasing the calcination temperature resulted in increasing the crystallite size of Mg–Cu–Zn ferrite powders. VSM measurement also indicated that the maximum saturation magnetization (64.1 emu/g) appears for sample calcined at 800 °C while there is not much further increase in M_s at higher calcination temperature. The value of coercivity field (H_c) presents a maximum value of 182.7 Oe at calcination temperature 700 °C. TEM micrograph of the sample calcined at 800 °C showed spherical nanocrystalline ferrite powders with mean size of 36 nm. The toroidal sample sintered at 900 °C for 4 h presents the initial permeability (μ_i) of 405 at 1 MHz and electrical resistivity (ρ) of 1.02×10^8 Ω cm.

Keywords MgCuZn ferrite · Sol–gel auto combustion · Nanocrystalline · Magnetic properties

M. R. Barati (✉)
Department of Materials Engineering, Faculty of Engineering, Monash University, Clayton, VIC 3800, Australia
e-mail: Mohammad.Barati@eng.monash.edu.au

1 Introduction

Recent interest in the study of several spinel type ferrites is in terms of the synthesis of their nanoparticles at low temperatures by different techniques, in view of the potential applications of these nanosized magnetic materials in different technological areas, as well as to study the intriguing magnetic properties of the nano-ferrite materials [1–6]. The magnetic properties of the nanosized ferrites are entirely different from those of their bulk counterparts, such as the superparamagnetic behavior and associated properties. Nanosized ferrites with uniform particle size and narrow size distribution are desirable for a variety of applications like targeted drug delivery, ferrofluids, medical imaging and other biomedical applications, magnetic data storage, etc., [7–11].

Among the different spinel-type ferrites, the Mg–Cu–Zn ferrite system is one of the most versatile, from the viewpoint of their large number of potential applications, due to their high resistivity, low dielectric loss, high Curie temperature, high permeability, low cost, etc., [12–14]. Present studies on this ferrite system is focused on the production of the nanosized materials at very low temperatures so that the nanosized material produced can be sintered at relatively lower temperatures, compared to the high temperatures required for materials synthesized by the conventional ceramic method. It is easy to obtain better dielectric properties, high performance parameters, and improved magnetic and related properties [12–14], for such materials. Better sinterability at low temperatures is desired in terms of saving energy as well as to minimize the loss of zinc during high-temperature sintering. In addition, the sintered Mg–Cu–Zn ferrite is usually used as magnetic material for MLCIs. These devices are fabricated by laminating ferrite layers and internal conductors alternately and then co-firing

to form the monolithic structure. Silver is usually used as the internal electrode material of MLCIs due to its high-conductivity and low cost. Silver (as internal conductor) has a melting point of 961 °C. Therefore, the ferrite powder needs to be sintered at <961 °C in order to co-fire with silver electrodes. Low-temperature sintering of Mg–Cu–Zn ferrite, therefore, is required for MLCI applications.

So, several wet chemical methods such as hydrothermal synthesis [15], combustion synthesis [16, 17], sol–gel techniques [18], citrate method [19, 20] and chemical coprecipitation method [21], have been developed for preparation of nanosized ferrites. However, all of these wet chemical methods, to some extent, still need calcination at relatively high temperatures and long soaking to obtain the final powders with expected crystal structure.

In our previous studies [22–24], a novel sol–gel auto-combustion method was developed to synthesize Ni–Zn and Ni–Cu ferrites nanocrystalline powders.

This is a novel way with a unique combination of the chemical sol–gel process and the combustion process. The process has advantages of inexpensive precursors, simple preparation and resulting nanocrystalline homogeneous powder.

In present study the sol–gel auto combustion preparation of Mg–Cu–Zn ferrite nanocrystalline powder, with chemical formula of $Mg_{0.17}Cu_{0.20}Zn_{0.63}Fe_2O_4$ was carried out using aqueous solution of ferric nitrate, magnesium nitrate, zinc nitrate, copper nitrate, citric acid and ammonia. The phase evolution during combustion and the subsequent calcination was also investigated. This method resulted in formation of single phase ferrite nanocrystalline powder after combustion and subsequent calcination which further characterized by DTA/TG, IR spectra, XRD, EDX, VSM, SEM and TEM techniques. Additionally, the initial permeability and electrical resistivity of sintered Mg–Cu–Zn ferrite are also described in this paper.

2 Experimental

Analytical grade magnesium nitrate [$Mg(NO_3)_2{\cdot}6H_2O$], zinc nitrate [$Zn(NO_3)_2{\cdot}6H_2O$], copper nitrate [$Cu(NO_3)_2{\cdot}3H_2O$], iron nitrate [$Fe(NO_3)_3{\cdot}9H_2O$] and citric acid [$C_6H_8O_7{\cdot}H_2O$] were used to prepare the ferrite compositions $Mg_{0.17}Cu_{0.20}Zn_{0.63}Fe_2O_4$. The specified amount of metal nitrate and citric acid was first dissolved in to deionized water to form the sol. The molar ratio of nitrates to citric acid was 1:1. Ammonia was also slowly added to the sol to adjust the pH value at about 7. During this procedure, the sol was continuously stirred by a magnetic agitator. Then, the sol was poured in to a dish and heated at 80 °C on a hot plate and stirred continuously till to transform into a xerogel. At a proper temperature ignition started and the dried gel burnt in a self-propagating combustion manner until all the gel was burnt out completely to form a fluffy loose powder. The entire combustion process was done in a few minutes. Finally, the as-burnt powders were calcined in the muffle furnace at 400–800 °C for 1 h with a heating rate of 10 °C/min to obtain the single phase ferrite. The powders calcined was granulated using a small amount of saturated solution of polyvinyl alcohol as a binder and was uniaxially pressed at a pressure of 1,300 kg/cm^2 for 1–2 min in a stainless steel die to form green toroidal and pellet specimens. After binder burnt out at 600 °C for 1 h, the specimens were sintered in the muffle furnace at 800 and 900 °C for 4 h in air atmosphere and cooled in the furnace. All specimens were heated slowly in the programmable muffle furnace to 550 °C at the rate of about 2 °C min^{-1} to avoid cracking of the specimens. Then, the temperature was raised to sintering temperature of 800 and 900 °C and kept at this temperature for 4 h. The cooling was done in the furnace at the rate of about 50 °C h^{-1} to 450 °C when the furnace was switched off. The surfaces of all the specimens were polished in order to remove any oxide layer formed during the process of sintering.

The autocatalytic nature of the combustion process has been studied by differential thermal analysis (DTA) and thermogravimetry (TG) analysis of the dried gel at a heating rate of 10 °C/min in static air.

Infrared spectra (IR) of the dried gel, as-burnt powder and calcined powder at 800 °C were recorded on a Bruker (Tensor 27) spectrophotometer from 400 to 4,000 cm^{-1} by the KBr pellet method.

The phase identification of the dried gel, as-burnt powder and calcined powders was performed by X-ray diffraction (XRD) on a Philips PW-1730 X-ray diffractometer using Cukα radiation ($\lambda = 1.5405$ Å). The average crystallite size of the synthesized powders was determined by X-ray line broadening technique using the well known Scherrer formula. The elemental composition of the calcined powders at 800 °C was analyzed by EDX analysis. The particle morphology of the calcined powders was studied with a transmission electron microscope (TEM). Vibrating sample magnetometer (VSM) with a maximum magnetic field of 10 kOe was carried out at room temperature to evaluate the magnetic properties of the calcined powders.

The bulk density and apparent porosity of sintered specimens was measured by Archimedes principle. The average grain size is obtained by measuring number of grains intersecting the straight line of the specific length in μm. This process of counting the number of grains is repeated for different positions on the micrographs and the data are averaged to get average grain size in μm. CamScan MV2300 scanning electron microscopy (SEM) was used to determine the microstructure of the sintered specimens.

The frequency dispersion of permeability was measured by using Impedance Analyzer. The resistivity of sintered Mg–Cu–Zn ferrite was measured on pellet specimens by applying silver electrodes on the surfaces.

3 Results and discussion

The experimental observation revealed that the nitrate–citrate gel, with the molar ratio 1:1, exhibit a self-propagating combustion behavior. Figure 1 shows the DTA and TG of the dried gel. It could be seen that there is an endothermic trough and three exothermic peaks in the DTA diagram. The endothermic trough at around 110 °C with a small weight loss (7%) seems to be due to the loss of residual water in the gels. The first sharp exothermic peak in the region of 200–228 °C in DTA diagram with a large weight loss of approximately 70% showing in TGA diagram corresponds to reaction between the nitrate and citric systems. This indicates that the decomposition of the gel occurs suddenly in a single step, as observed in the other systems [22, 25]. The weight loss associated with this exothermic reaction probably attributed to the exit of water steam, H_2, NO_x ($x = 1, 2$) and CO_2. Therefore, the combustion could be considered as a thermally induced anionic, redox reaction of the gel wherein the citrate ions act as reductant and nitrate ions act as oxidant. Since the nitrate ions provide an in situ oxidizing environment for the decomposition of the organic component, the rate of oxidation reaction increases slightly. The combination of the lowering of the reaction temperature and the increase in rate results in a self-propagating combustion of the nitrate–citrate gel [22–24]. The second exothermic peak at about 375 °C with a weight loss of 18% corresponds likely to the burning of un-reacted starting citric acid remaining after combustion. The last broadened exothermic peak at about 590 °C with a weight loss of 5% corresponds to the crystallization of spinel phase.

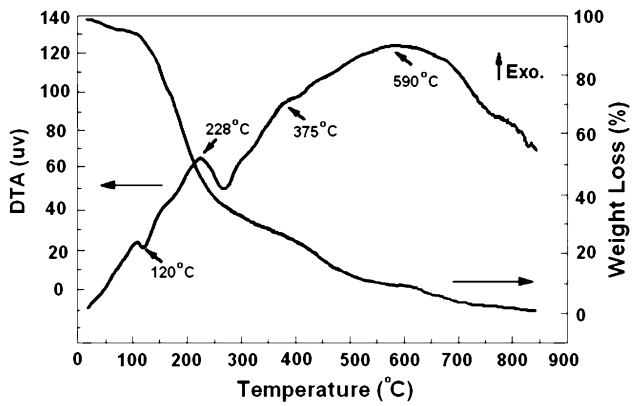

Fig. 1 DTA and TG plots for the dried nitrate–citrate gel

Chemical and structural changes, and the desired crystal phases present in the materials during combustion and calcination processes could be observed by characterization using different kind of spectrometers. This may be helpful in understanding the combustion reaction mechanism.

Figure 2 shows IR spectra of dried gel, as-burnt powder and calcined powder at 800 °C in the range 400–4,000 cm^{-1}. It is clearly seen from the Fig. 2a that the dried gel show several absorption bands at about 3,151, 1,632 and 1,370 cm^{-1} corresponding to the hydroxyl group, carboxyl group and NO_3^- ions, respectively. The appearance of the characteristic bands of NO_3^- indicates that the NO_3^- exists as a group in the structure of citrate gel during the gelation of mixed solution formed from nitrates and citric acid. In the IR spectrum curve of the powder after combustion (Fig. 2b) the absorption band at $\sim$1,370 cm^{-1}, which corresponds to NO_3^- ions, disappears and the bands at $\sim$1,632 and 3,151 cm^{-1} which correspond to the carboxyl group and hydroxyl group decrease significantly. On the other hand, a significant spectroscopic band at $\sim$570 cm^{-1} appears which seems to be the characteristic absorption band of ferrite. This decrease of the characteristic bands of carboxyl group and NO_3^- ions suggests that carboxyl group and NO_3^- ions take part in a reaction during combustion. Therefore, the combustion is an exothermic reaction in the dried gel where nitrate ions act as oxidant and carboxyl group is reductant as observed in the other systems [14, 22,

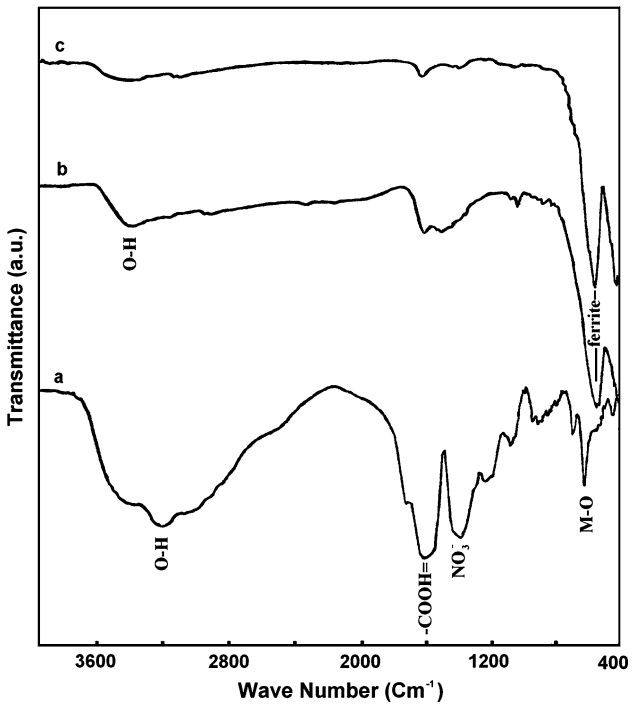

Fig. 2 Typical IR spectra of **a** the dried gel, **b** as-burnt powder, **c** calcined powder at 800 °C

23]. In the IR spectrum curve of the powder calcined at 800 °C (Fig. 2c) it can be seen that characteristic bands of carboxyl group disappeared and only one absorption band at ~570 cm^{-1} existed which correspond to the single phase ferrite.

To aid further interpretation of the reaction processes, the DTA/TGA and IR spectra analysis was supplemented by XRD analysis. Figure 3 shows the XRD patterns of dried gel, as-burnt powder and powders calcined at various temperatures. The dried gel is amorphous in nature (Fig. 3a). The heat released in the process of exothermic decomposition has been observed to be sufficient for complete conversion of the metal compounds to metal oxides. The XRD pattern of the as-burnt powder (Fig. 3b) indicates the presence of $Mg_{0.17}Cu_{0.20}Zn_{0.63}Fe_2O_4$ as a major phase and Fe_2O_3 (hematite) as a minor phase. The XRD patterns of the powders calcined at various temperatures (Fig. 3c–f) shows that with increasing the calcination temperature the amount of Fe_2O_3 decreases markedly. The completion of the formation of single phase $Mg_{0.17}Cu_{0.20}Zn_{0.63}Fe_2O_4$ ferrite occurred at 800 °C. Thus, the calcination temperature which is required to obtain single-phase Mg–Cu–Zn ferrite is 800 °C. This temperature is relatively low, compared to that of synthesized by the conventional solid-state reaction method which is reported above 1,050 °C [26]. The (hkl) values corresponding to the diffraction peaks of spinel phase are marked in the Fig. 3f. The XRD pattern also shows that the peaks become sharper with increasing of calcination temperature. It implies progressive growth of crystallites after calcination at higher temperatures. The crystallite size of the calcined powders at various temperatures was calculated from the full-width at half-maximum (FWHM) of the strongest diffraction peak (113) using the Scherrer formula [22–25]. Table 1 shows comparative average crystallite size of the synthesized powders as a function of calcination temperature. The crystallite size of single-phase ferrite is about 36 nm. It could be seen that the crystallite sizes increases with increasing the calcination temperature, which can be due to higher growth rate in high temperatures.

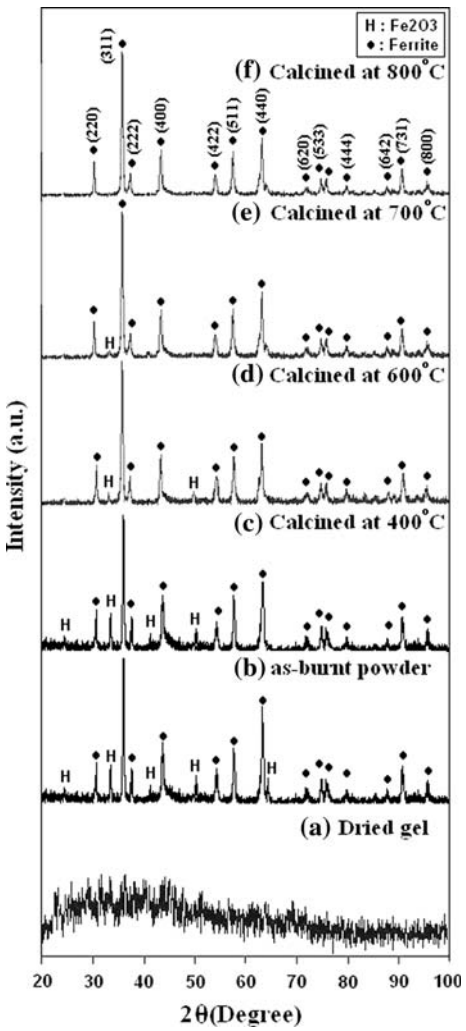

Fig. 3 XRD patterns of **a** dried gel, **b** as-burnt powder and powders calcined at **c** 400 °C, **d** 600 °C, **e** 700 °C and **f** 800 °C for 1 h

The cubic lattice parameter obtained for the powder calcined at 800 °C ($a = 8.471$ Å) is comparable to that of the bulk ferrite (8.484 Å). The slightly smaller value of the lattice parameter of the nanoferrite is a common feature observed for nanosized ferrites, due to the lattice contraction in fine particles, as well as due to a difference in the distribution of the different metal ions in the A and B sites of the spinel structure [25].

Chemical analyses through EDX were also carried out on powder calcined at 800 °C. The EDX analysis shows the wt% of magnesium, copper, zinc and iron in the powder calcined at 800 °C is 1.76, 5.43, 17.62 and 47.78 wt%, respectively, which are in coincidence with the wt% of magnesium, copper, zinc and iron in phase $Mg_{0.17}Cu_{0.20}Zn_{0.63}Fe_2O_4$ ferrite; as this phase is the detected from the XRD pattern (Fig. 3f). The result of EDX area analysis confirms the XRD result.

Table 1 Magnetic properties and crystallite size (average ± standard deviation) for the powders calcined at 400, 600, 700, 800 and 900 °C for 1 h

Calcination temperature (°C)	Saturation magnetization (M_s) (emu/g)	Remanence (M_r) (emu/g)	Coercivity (H_c) (O_e)	Crystallite size (nm)
400	29.5	13.5	100.4	28 ± 5.2
600	38.5	16.1	147.6	30.5 ± 5.4
700	55.3	22.3	182.7	33 ± 5.6
800	64.1	28.3	85.1	36 ± 5.1
900	66.8	30.1	51.5	40 ± 4.9

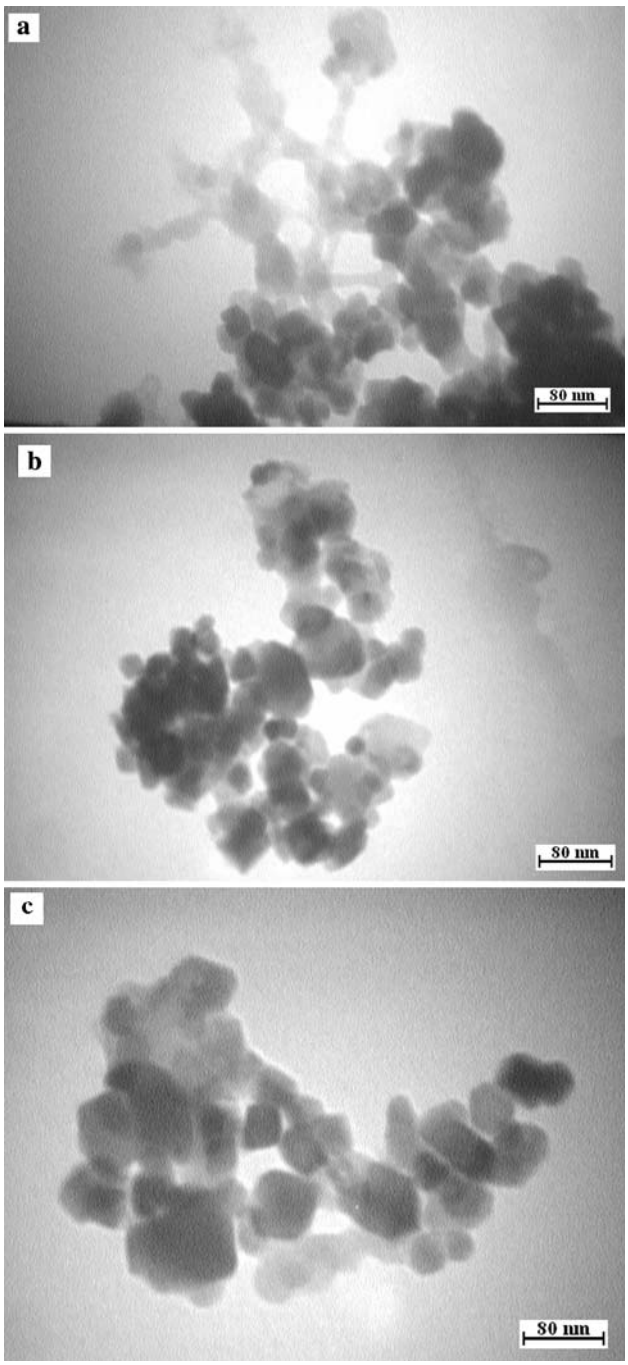

Fig. 4 TEM micrograph of **a** as-burnt powder and calcined powders at **b** 700 °C and **c** 800 °C for 1 h

Figure 4 shows the TEM micrographs of the as-burnt powder and calcined powders at 700 and 800 °C. The as-burnt powder indicates the co-existence spherical particles with an average particle size of 22 nm and small amount of residual dried gel after combustion (Fig. 4a). This implies the incomplete decomposition of dried gel during combustion. The calcined powders also exhibit homogeneous morphology of the cubic ferrite nano particles. The average particle size dramatically increases from 33 to 36 nm on increasing the calcinations temperature from 700 to 800 °C (Fig. 4b, c). The average particle size derived from TEM measurement is in good agreement with the average crystallite size obtained from line broadening Scherrer formula in Table 1.

Since the calcination temperature has a significant effect on the morphology and the phase constitution of the products, it strongly determines the magnetic properties of the powders. Figure 5 shows the magnetization curves of the powders calcined at 400, 600, 700, 800 and 900 °C for 1 h, measured at room temperature. The magnetic data are tabulated in Table 1. The value of coercivity field (H_c) firstly increases as the calcination temperature increases and then declines rapidly with further increasing calcination temperature whereas the saturation magnetization continuously increases. Maximum coercivity (182.7 Oe) is obtained for the sample calcined at 700 °C with particle size of 33 nm (see Fig. 4) which could be considered as critical diameter for single-domain Mg–Cu–Zn ferrite particle. It was known that there was no domain wall in the single-domain particles. The magnetization mechanism was a domain rotation process. The H_c was in direct proportion to the size of single-domain particles [26–28]. Therefore, H_c gradually increased with the size of single-domain particles (below 700 °C). However, when the size arrived to the critical diameter of a single domain, the coercivity started decreasing because of the change from single domain to a multi-domain structure. Relatively low values of coercivity of the sample calcined at 800 and 900 °C may be originated from the multi domain nature of the nano particles due to their large size. The multi-domain behavior and therefore the mechanism of magnetization reversal by domain wall motion explain the reduced coercivity observed for these samples. Similarly, the saturation magnetization reaches a maximum value of 64.1 emu/g for the sample calcined at 800 °C and there is not much further increase in M_s, when calcined above this temperature (900 °C). The presence of phase such as Fe_2O_3 is the main reason for the low magnetic properties at 400 and 600 °C. The observed improvement in M_s by calcination is believed to be due to the more complete crystallization of the ferrite phase and the enhancement in crystallinity of the ferrite phase nano particles. Another important factor related to improvement of M_s is the elimination of Fe_2O_3 phase. The VSM results are correlated well with the results obtained from XRD, EDX and TEM. It could be concluded that increasing the calcination temperature is beneficial to eliminate the intermediate phases and form single-phase ferrite and enhance the magnetic properties.

The calcined powders at 800 °C was uniaxially pressed under the pressure of 1,300 kg/cm^2 for 1–2 min in a stainless steel die to form green toroidal and then sintered

at in the muffle furnace at 800 and 900 °C for 4 h in air atmosphere.

Figure 6 shows the SEM microphotograph of the Mg–Cu–Zn ferrite sintered at 800 and 900 °C for 4 h. It is clearly seen that densified ferrite with a fine-grained microstructure behavior can be prepared at <950 °C by using gel-derived nanocrystalline powder. The average grain size is about 0.87 μm with standard deviation of 0.07 μm for specimen sintered at 800 °C, whereas for specimen sintered at 900 °C average grain size is about 0.98 μm with standard deviation of 0.09 μm. The Mg–Cu–Zn ferrite powder with the same composition, synthesized by the conventional solid-state reaction method, can be sintered only at temperatures above 1,050 °C [26]. So, the synthesized nano-sized powder exhibits highly reactive behavior, and can be sintered at <950 °C without any low-melting-point additives. This is of importance for the high-performance MLCIs, because the low-melt additives in low-temperature sintered ferrites are usually detrimental to the reliability of MLCIs. The high activity of the synthesized powder may originate from the nanometer scale particle size.

The bulk density, percentage porosity, electrical resistivity and initial permeability of sintered specimens at 800 and 900 °C are also tabulated in Table 2. From Table 2, it is seen that the bulk density and initial permeability increases with increasing sintering temperature, while the percentage porosity and electrical resistivity decreases with increasing the sintering temperature, indicating improved densification with increasing sintering temperature. It can be noticed from Table 2 that Mg–Cu–Zn ferrite possesses good electromagnetic properties, similar to those of the low-temperature sintered Ni–Cu–Zn ferrites [14]. All electromagnetic properties fulfill the requirements of MLCI. Therefore, the synthesized Mg–Cu–Zn ferrite can be used as a magnetic material for MLCIs. The initial permeability was found increases with increasing sintering temperature from 800 to 900 °C. Increase in permeability can be attributed to increase in grain size with sintering temperature [29]. Globus et al. [30] and Costa et al. [29] investigated several NiZn ferrites and found a linear relationship between permeability and grain size. Perduijn et al. [31] and Roess et al. [32] also studied the effect of grain size on the initial permeability and found a linear relation between the initial permeability and grain size in MnZn ferrites. They believed the relationship between μ_i and grain size could be expressed by means of the following relation:

$$\mu_i \propto \frac{M_S^2 D}{K_1} \tag{1}$$

where M_s is the saturation magnetization, D is the average grain size, K_1 is the anisotropy constant which is proportional to the magnetic domain wall energy. Larger grains tend to consist of a greater number of domains walls. In this case, the increase in initial permeability occurred owing to easy reversible displacement or domain wall movement in the direction of the applied magnetic field. For this displacement to occur, the energy of the applied external field must be greater than the domain wall pinning. Therefore, the easier the displacement, the greater the initial permeability. The second reason could be related to the increase in bulk density and decrease in porosity of the sintered ferrite with increasing sintering temperature. It is known that ferrites with higher density and lower porosity possess a higher initial permeability. The presence of pores reduces the

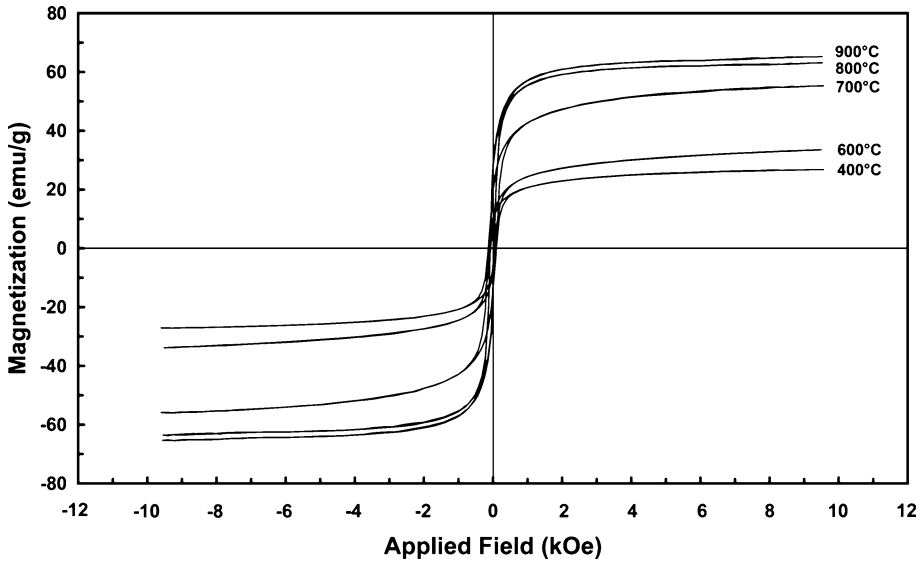

Fig. 5 Magnetization curves for powders calcined at 400, 600, 700, 800 and 900 °C for 1 h

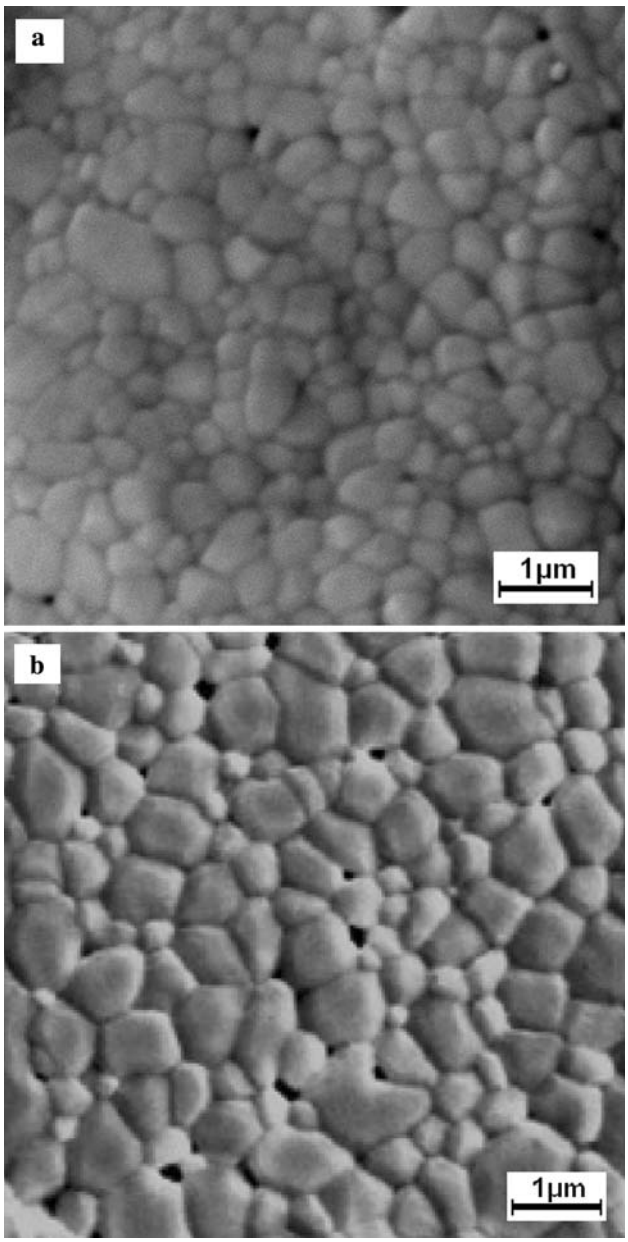

Fig. 6 SEM micrographs of sintered specimens at **a** 800 °C and **b** 900 °C for 4 h

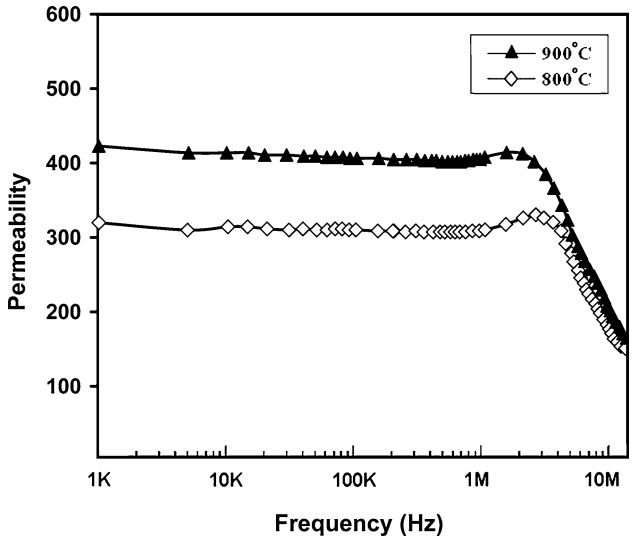

Fig. 7 Frequency dependence of initial permeability for the specimens sintered at 800 and 900 °C for 4 h

permeability due to increase in the demagnetizing field. The presence of intragranular pores provides the impediment to the domain wall displacement and causes decrease in permeability.

Figure 7 also shows initial permeability as a function of frequency in the range 1 kHz–13 MHz for samples sintered at 800 and 900 °C. The initial permeability shows flat profile within the frequency range 1 kHz–3 MHz, indicating good high frequency stability and then its dispersion occurs. In general, it is observed that the initial permeability remains almost constant up to certain lower range of frequency after which the initial permeability increases to a maximum value and then decreases rapidly to a very low value. It is known that the permeability of polycrystalline ferrite can be described as the superposition of domain wall motion and spin rotation components. At the low frequency range of 10 kHz–1 MHz, domain wall motion plays a predominant role in the magnetizing process and loss mechanism. The high permeability value at low frequencies shows the dominant role played by domain wall motion. For the specimens sintered at 800 and 900 °C wall relaxation occurs in the 2 MHz range.

4 Conclusions

Nanocrystalline Mg–Cu–Zn ferrite was synthesized by sol–gel auto-combustion. The nitrate–citrate gels exhibit a

Table 2 Bulk density (mean ± standard deviation), percentage porosity (P), electrical resistivity (ρ) and initial permeability (μ_i) of sintered specimens at 800 and 900 °C for 4 h

Sintering temperature (°C)	Bulk density (g/cm^3)	Percentage porosity (%)	Electrical resistivity ($\times 10^8$ Ω cm)	μ_i	
				10 kHz	1 MHz
800	4.78 ± 0.32	6.44	1.06	315	309
900	4.81 ± 0.36	5.51	1.02	414	405

self propagating behavior after ignition in air. The results show that with the sol–gel auto-combustion technique it is possible to synthesized the ferrites at relatively lower temperatures and much shorter duration than that required in the conventional solid-state route. The saturation magnetization increases with increasing sintering temperature and a maximum value of 64.1 emu/g is obtained after calcination at 800 °C. The experiments conducted in this study suggest that the sol–gel auto-combustion process is an effective and convenient route to synthesize nanocrystalline Mg–Cu–Zn ferrite particles because there is no requirement for a calcination process at high temperature. The synthesized powder has high activity due to its nano-sized particle size. The ferrite powder can be sintered at 900 °C, and possesses a fine-grained microstructure. The low-temperature sintered Mg–Cu–Zn ferrite has good electromagnetic properties, which makes this material suitable for MLCI applications.

Acknowledgments The author would like to express their thanks to Mr. Yourdkhani and Mr. Nikkhah-Moshaie for useful helps and discussions.

References

1. Dyal A, Loos K, Noto M et al (2003) J Am Chem Soc 125:1684
2. Choi EJ, Ahn Y, Kim S et al (2003) J Magn Magn Mater 262:L198
3. Sinha A, Nayar S, Murthy GVS et al (2003) J Mater Res 18:1309
4. Caizer C, Stefaneson M (2002) J Phys D Appl Phys 35:3035
5. Hrianca I, Caizer C, Schlett Z (2002) J Appl Phys 92:2125
6. Liu C, Zou B, Rondinone AJ et al (2000) J Am Chem Soc 122:6263
7. Shinkai M (2002) J Biosci Bioeng 94:606
8. Lubbe AS, Alexiou C, Bergemann C (2001) J Surg Res 95:200
9. Tiefenauer LX, Tschirky A, Kuhne G et al (1996) Magn Reson Imaging 14:391
10. Skmoski R (2003) J Phys Condens Matter 15:R841
11. Gibbs MRJ, Opin C (2003) Solid State Mater Sci 7:83
12. Yue Z, Zhou J, Wang X et al (2001) Mater Sci Eng B86:64
13. Qi X, Zhou J, Yue Z et al (2002) J Magn Magn Mater 251:316
14. Yue Z, Zhou J, Wang X et al (2001) J Mater Sci Lett 20:1327
15. Jiao X, Chen D, Hu Y (2002) Mater Res Bull 37:1583
16. Hwang C, Tsai J, Huang T (2005) J Mater Chem Phys 110:1
17. Peng CH, Hwang C, Chen S (2004) J Mater Sci Eng 107:295
18. Chen DH, He XR (2001) Mater Res Bull 36:1369
19. Mouallem-bahout M, Bertrand S, Pena O (2005) J Solid State Chem 178:1080
20. Verma A, Goel TC, Mendiratta RG et al (2000) J Magn Magn Mater 208:13
21. Chen Q, Rondinone AJ, Chakoumakos BC et al (1999) J Magn Magn Mater 194:1
22. Barati MR, Seyyed Ebrahimi SA, Badiei A (2008) Key Eng Mater 368–372:598
23. Barati MR, Seyyed Ebrahimi SA, Badiei A (2008) Mod Phys B22:3153
24. Azadmanjiri J, Salehani HK, Barati MR et al (2007) J Mater Lett 61:84
25. Deka S, Joy PA (2006) Mater Chem Phys 100:98
26. Rezlescu N, Rezlescu E, Popa PD et al (1998) J Magn Magn Mater 182:199
27. Huang Y, Tang Y, Wang J et al (2006) Mater Chem Phys 97:394
28. Zhang HE, Zhang BF, Wang GF et al (2007) J Magn Magn Mater 312:126
29. Costa ACFM, Tortella E, Morelli MR et al (2003) J Magn Magn Mater 256:174
30. Globus A, Duplex P, Guyot M (1971) IEEE Trans Magn 7:617
31. Perduijin DJ, Peloschek HP (1968) Proc Br Ceram Soc 10:263
32. Manjurul HM, Huq M, Hakim MA (2008) J Phys D Appl Phys 41:55007